Consistent Higher-Order Transport Models for SOI MOSFETs

Martin Vasicek*, Johann Cervenka*, Markus Karner†, and Tibor Grasser†
*Institute for Microelectronics, TU Wien
†Christian Doppler Laboratory for TCAD at the Institute for Microelectronics, TU Wien
Gußhausstraße 27–29/E360, A–1040 Wien, Austria
Email: {vasicek|cervenka|karner|grasser}@iue.tuwien.ac.at

***Abstract*—We have developed a two-dimensional non-parabolic macroscopic transport model up to the sixth order. To model higher-order transport parameters with as few simplifying assumptions as possible, we apply an extraction technique from Subband Monte Carlo simulations followed by an interpolation within these Monte Carlo tables through the whole inversion layer. The impact of surface-roughness scattering as well as quantization on the transport parameters is inherently considered in the Subband Monte Carlo data. These tables are used to model higher-order mobilities as well as the macroscopic relaxation times as a function of the effective field and the carrier temperature. We have studied the influence of the inversion layer concentration on higher-order transport parameters within high fields and show the behavior of these parameters in a quantized system of a UTB SOI MOSFET.**

I. Introduction

For engineering applications macroscopic transport models based on Boltzmann's transport equation (BTE) like the drift-diffusion (DD) model or the energy transport model (ET) are very efficient compared to the time consuming Monte Carlo (MC) simulation [1]. However, with further decrease of the device dimensions into the deca-nanometer regime both the DD, and the ET model become more and more inaccurate [2]. Investigations have demonstrated [3, 4] that higher-order macroscopic models can cover the gate length range of $100\,\mathrm{nm}$ down to about $25\,\mathrm{nm}$. In the analysis of macroscopic models up to the sixth order, it is essential to describe the transport parameters, namely the carrier mobility μ_0, the energy-flux mobility μ_1, the energy relaxation time τ_1, the second-order energy-flux mobility μ_2, and the second-order energy relaxation time τ_2 with as few simplifying assumptions as possible. A rigorous study of the behavior of these parameters in the bulk case has been already carried out using bulk MC tables [3]. The use of this bulk data set for modeling transport in MOSFET devices is problematic due to the importance of surface roughness scattering and quantization in the inversion channel. In [5] surface roughness scattering on the carrier mobility has been investigated using the semiempirical Matthiesen rule, but a rigorous study has not been performed yet.

In order to take these important inversion layer effects as well as non-parabolic bands for high fields into account, we have developed a Subband Monte Carlo (SMC) [6, 7] table based 2D electron gas six moments transport model. It is now possible to study the influence of the inversion layer effects on higher-order transport parameters.

II. Model

In order to derive 2D higher-order macroscopic models like the six moments model one has to multiply the BTE

$$\partial_t f + \mathbf{v} \cdot \nabla_{\mathrm{r}} f - \frac{\mathbf{F}}{\hbar} \cdot \nabla_{\mathrm{k}} f = \left(\partial_t f\right)_{\mathrm{coll}} \ , \tag{1}$$

with special weight functions [8] and integrate over the $\mathbf{k}$-space. $f(\mathbf{r}, \mathbf{k}, t)$ is the distribution function, $\mathbf{F}$ is the driving force, and $\mathbf{v}(\mathbf{k})$ is the group velocity in the BTE. The moments in 2D space are defined as

$$x(\mathbf{r}, t) = \frac{2}{(2\pi)^2} \int_0^\infty X(\mathbf{k}) f(\mathbf{r}, \mathbf{k}, t) \mathrm{d}^2 k = n(\mathbf{r}, t) \langle X(\mathbf{k}) \rangle \ , \tag{2}$$

with $x(\mathbf{r}, t)$ as the macroscopic values together with the microscopic counterpart $X(\mathbf{k})$. $n(\mathbf{r}, t)$ is the carrier concentration. Substituting the microscopic weights with $\epsilon^i(\mathbf{k})$ and $\mathbf{v}(\mathbf{k})\,\epsilon^i(\mathbf{k})$ one will obtain the even, scalar-valued moments, and the odd, vector-valued moments, respectively. For the six moments model i is in the range of $i \in [0, 2]$. The scattering operator of the BTE is modeled using the macroscopic relaxation time approximation [9]. For the even moments the macroscopic relaxation time ansatz looks like

$$\partial_t \langle X \rangle_{\mathrm{coll}}^{\mathrm{even}} \approx -n \frac{\langle \epsilon^i \rangle - \langle \epsilon^i \rangle_0}{\tau_i} \ , \tag{3}$$

and for the odd moments

$$\partial_t \langle X \rangle_{\mathrm{coll}}^{\mathrm{odd}} \approx -n \frac{\langle \mathbf{v} \epsilon^i \rangle}{\tau_i} \ . \tag{4}$$

$\langle \epsilon^i \rangle_0$ are the even moments in equilibrium. Further approximations during the derivation are the diffusion approximation, which states that the anti-symmetric part of the distribution function is much smaller than the symmetric one [10], the modeling of the tensorial components, and the closure relation [11]. The transport model will be formulated in terms of $w_i = \langle \epsilon^i \rangle$ and $\mathbf{V}_i = \langle \mathbf{v} \epsilon^i \rangle$ [3]. The general conservation equation reads

$$\partial_t \left(n w_i\right) + \nabla \cdot \left(n \mathbf{V}_i\right) - i \mathbf{F} \cdot n \mathbf{V}_{i-1} = -n \frac{w_i - w_{i,eq}}{\tau_i} \ , \tag{5}$$

978-1-4244-1753-7/08/$25.00 ©2008 IEEE

whereas the general fluxes are defined as

$$n\mathbf{V}_i = -\frac{\mu_i H_{i+1}}{2\mathrm{q}}\left(\nabla\left(nw_{i+1}\right) - n\mathbf{F}w_i\frac{2+iH_i}{H_{i+1}}\right). \quad (6)$$

H_i are the non-parabolicity factors, and are defined in the 2D space as

$$U_i = \frac{1}{2}\mathrm{tr}\left(\hat{\mathrm{U}}_i\right) = \frac{1}{2}w_i H_i\,, \quad (7)$$

with $\hat{\mathrm{U}}_i = \langle \mathbf{v}\otimes\mathbf{p}\epsilon^i\rangle$ as the energy tensors [11]. The even moments w_i of the six moments model are expressed as $\mathrm{k_B}T_n$, $2\left(\mathrm{k_B}T_n\right)^2\beta$, and $6\left(\mathrm{k_B}T_n\right)^3\beta^c$. β is the kurtosis and denotes the deviation from a heated Maxwellian distribution function

$$\beta = \frac{1}{2}\frac{w_2}{w_1^2}\,. \quad (8)$$

c is an integer in the range $c \in [0, 3]$ [3]. To take the quantization as well as surface roughness scattering into account we extract the transport parameters τ_i and μ_i from a self-consistent coupling between a SMC simulator and a Schrödinger-Poisson (SP) solver. In the SMC simulator we consider non-parabolic bands, quantization effects, phonon induced scattering as well as surface roughness scattering [6, 12]. The SP solver incorporates the quantum confinement in inversion layers. Our device simulator Minimos-NT [13] calculates the effective field through the channel of a device and extracts higher-order transport parameters from the SMC tables. The mobilities as well as the relaxation times are now a function of the effective field and the carrier temperature $\mu_{\mathrm{i}}(E_{\mathrm{eff}}, T_n)$, $\tau_{\mathrm{i}}(E_{\mathrm{eff}}, T_n)$.

III. Results

As an example device a fully depleted SOI MOSFET with a Si film thickness of $4\,\mathrm{nm}$ in $\langle 100\rangle$ direction, and a donor doping concentration of $10^{20}\,\mathrm{cm}^{-3}$ in the source and the drain regions, and with an acceptor doping in the channel of $10^{16}\,\mathrm{cm}^{-3}$ has been investigated. An electric field is applied in $\langle 010\rangle$ direction.

In Fig. 1 we show higher-order mobilities as a function of the inversion layer concentration $\mathrm{N_{Inv}}$. We point out that in bulk MOSFETs for the low-field case the mobility of our simulation fits the measurement data of Takagi [14] while a significant reduction is observed in the quantized 4 nm channel region [15]. Furthermore it is demonstrated that for high lateral fields and high $\mathrm{N_{Inv}}$ the mobilities converge to the same value. This is not the case for the relaxation times. In Fig. 2 and Fig. 3 the energy relaxation times and the second-order energy relaxation time as a function of $\mathrm{N_{Inv}}$ are plotted for different lateral fields, respectively. For high $\mathrm{N_{Inv}}$ and for low fields the relaxation times increase compared to the high lateral field case where the relaxation times are constant. This can be explained with Fig. 4 where the first subband occupation as a function of $\mathrm{N_{Inv}}$ of the unprimed, primed, and double primed valley for lateral fields of $50\,\mathrm{kV/cm}$, and $200\,\mathrm{kV/cm}$ is shown. Due to the fast increase of the occupation number of the first subband in the unprimed valley at $50\,\mathrm{kV/cm}$ compared to the high-field case, where the occupation is constant, the change in

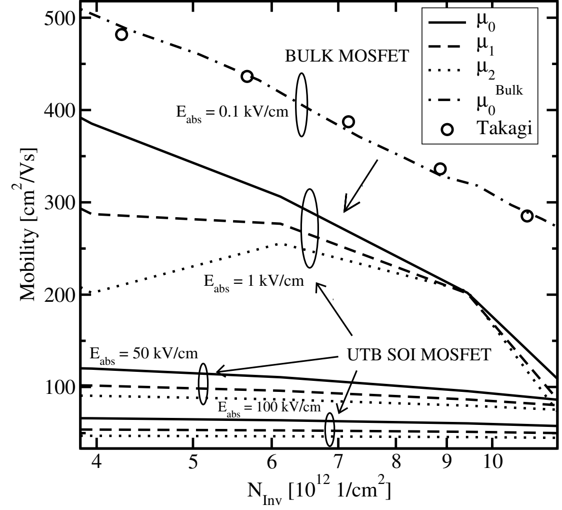

Fig. 1: The higher-order mobilities as a function of the inversion layer concentration $\mathrm{N_{Inv}}$ for different lateral fields $\mathrm{E_{abs}}$ are plotted. For high fields the difference of the mobilities decreases. For low fields in a bulk MOSFET the carrier mobility is equal to the measurement data of Takagi.

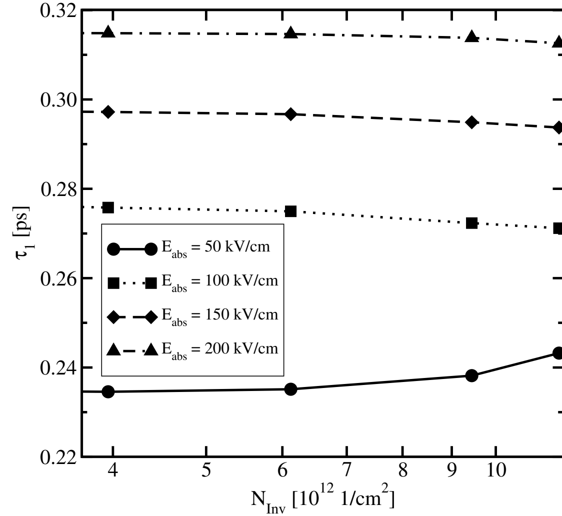

Fig. 2: The energy relaxation time as a function of the inversion layer concentration for different lateral fields is shown. For a field of $50\,\mathrm{kV/cm}$ and a high $\mathrm{N_{Inv}}$, τ_1 increases compared to high-fields, where the energy relaxation time is more or less constant.

the higher-order relaxation times increases as well for high N_{Inv}. Fig. 5 shows effective fields for different bias points through an SOI MOSFET with a gate length of $40\,\mathrm{nm}$. With the effective fields and the SMC tables one can model higher-order transport parameters through a device, as presented in Fig. 6. A profile of the carrier, the energy-flux, and the second-order energy flux mobilities has been pointed out. Fig. 7 is a comparison of the carrier temperature with the second-order temperature $\theta = \beta T_n$. The deviation of these two temperatures increases for high drain voltages due to the deviation of the distribution function from a Maxwellian distribution. The maximum peak is at the channel drain junction where hot electrons from the channel meet cold electrons from the drain.

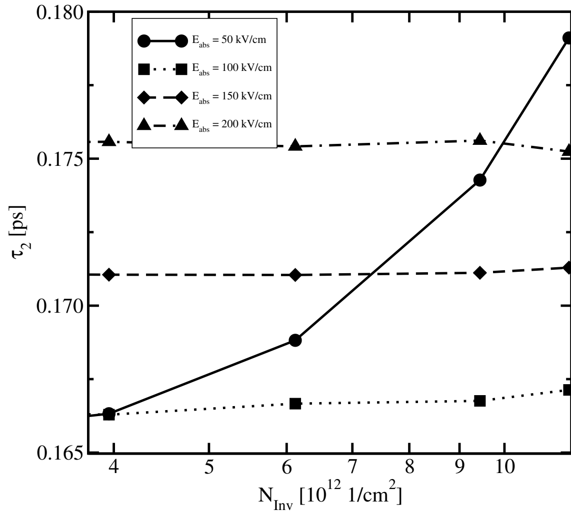

Fig. 3: The second-order relaxation time is shown as a function of the inversion layer concentration for different lateral fields. The increase of τ_2 at $50\,\mathrm{kV/cm}$ is as well higher than at the other fields. The change at high N_{Inv} and low fields of the second-order relaxation time compared to the other fields is higher than in the energy relaxation time.

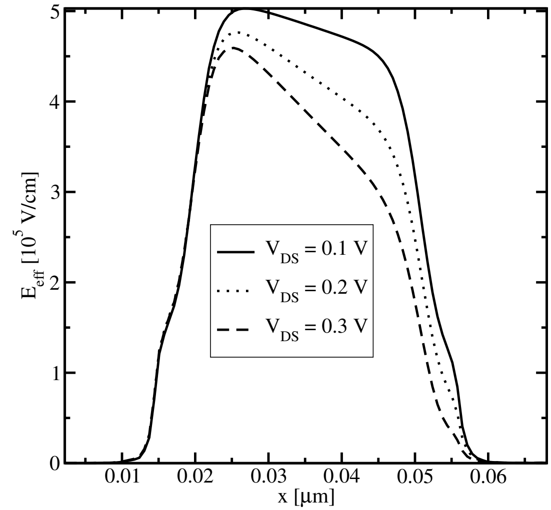

Fig. 5: The effective field throughout the whole device for drain voltages of $0.1\,\mathrm{V}$, $0.2\,\mathrm{V}$, and $0.3\,\mathrm{V}$. With the effective field and an interpolation between SMC tables, higher-order transport parameters can be modeled throughout the whole device.

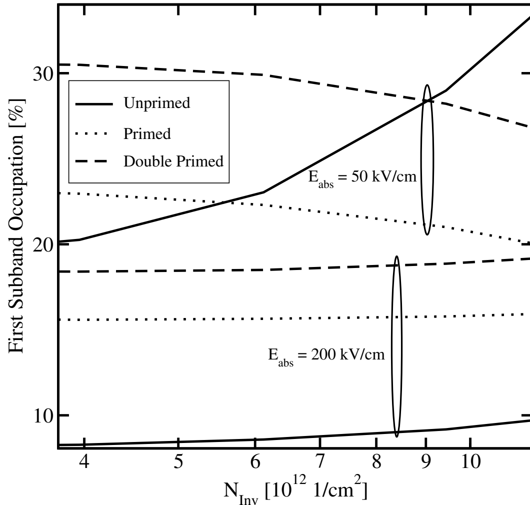

Fig. 4: The first subband occupation of the unprimed, primed, and double primed valley as a function of the inversion layer concentration for fields of $50\,\mathrm{kV/cm}$ and $100\,\mathrm{kV/cm}$. Due to the light mass of the unprimed valley in transport direction the subband occupation number is higher than in the other valleys.

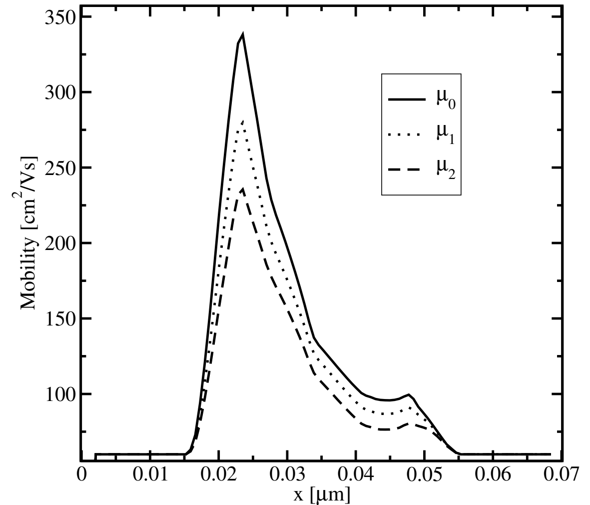

Fig. 6: The carrier, the energy-flux as well as the second-order energy flux mobilities are plotted through a $40\,\mathrm{nm}$ gate length SOI MOSFET. A drain voltage of $0.3\,\mathrm{V}$ has been applied.

Fig. 8 shows velocity profiles calculated with the DD, ET, and the six moments (SM) models of an SOI MOSFETs with a gate lengths of $40\,\mathrm{nm}$ and $60\,\mathrm{nm}$. In the $40\,\mathrm{nm}$ device the ET model considerably overestimates the velocity (and thus the drain current) with a velocity three times as high as the DD model, whereas for the $60\,\mathrm{nm}$ device it is just two times as high [2]. For large devices the velocity of the ET and the SM converge to the value of the DD model. In Fig. 9 we point out that with further increase of the gate lengths the difference between the output currents decreases. For large devices all transport models yield the same result.

IV. Summary and Conclusion

We have studied the behaviour of higher-order transport parameters in inversion layers. A method based on an interpolation between SMC tables for modeling a two-dimensional electron gas has been developed. This approach allows the investigation of UTB SOI devices including the influence of surface-roughness scattering and quantization within higher-order moment models. A generalized set of equations has been used to derive a novel 2D six moments model. First the influence of different inversion layers on higher-order transport parameters within high fields has been shown. We

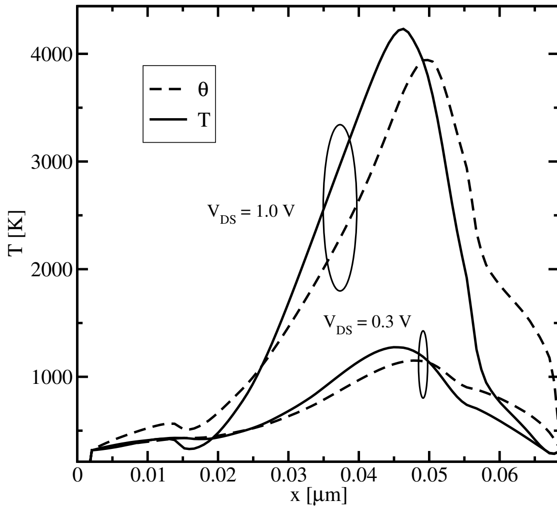

Fig. 7: The second-order temperature $\theta = \beta T_n$ in comparison to the carrier temperature T_n for $V_{\mathrm{DS}} = 0.3\,\mathrm{V}$ and $V_{\mathrm{DS}} = 1.0\,\mathrm{V}$. The deviation of the two temperatures has its maximum in the drain region, where the hot electrons from the channel meet cold electrons in the drain region. The difference of θ and T_n for $V_{\mathrm{DS}} = 1.0\,\mathrm{V}$ is higher than at $V_{\mathrm{DS}} = 1.0\,\mathrm{V}$.

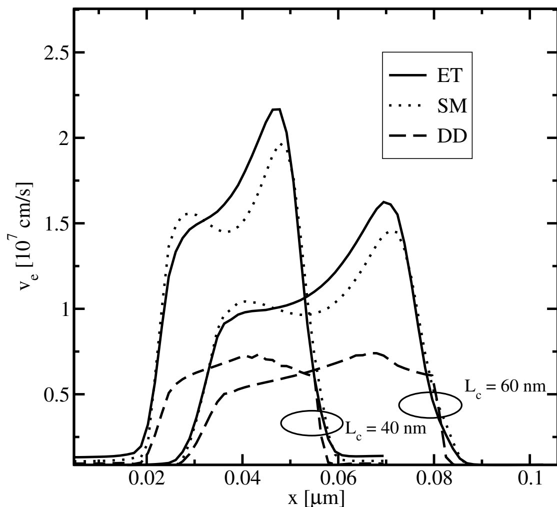

Fig. 8: Velocity profile calculated with the DD, ET, and the SM model for a 40 nm and 60 nm device. The velocity of the ET and SM model is smaller in the 60 nm than in the 40 nm device. DD predicts velocities independent from the gate length. Due to the quantization and surface roughness scattering the velocity in the DD model is smaller than the saturation velocity ($\approx 10^7\,\mathrm{cm/s}$) in the bulk.

found a significant change in the relaxation times for high inversion layer concentrations and low fields compared to high fields. Furthermore higher-order mobilities converge for high inversion layer concentrations to the same value. Second we have pointed out the importance of using higher-order moment models for the modeling of devices with a gate length in the deca-nanometer regime.

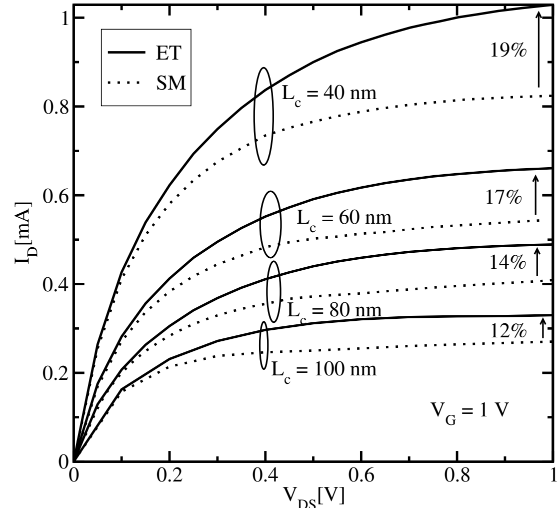

Fig. 9: Output characteristics calculated with the ET and the SM model for SOI MOSFETs with 40 nm, 60 nm, 80 nm, and 100 nm gate lengths. A gate voltage of $1\,\mathrm{V}$ is applied. For long channel devices the ET and the SM model yield the same result.

V. Acknowledgement

This work has been supported by the Austrian Science Fund project P18316-N13.

References

[1] F. Gamiz *et al.*, "Monte Carlo Simulation of Electron Transport Properties in Extremely Thin SOI MOSFET's," **45**(5), 1122 (1998).

[2] T. Grasser *et al.*, "Advanced Transport Models for Sub-Micrometer Devices," in *Proc. SISPAD* (2004) 1–8.

[3] T. Grasser *et al.*, "Nonparabolic Macroscopic Transport Models for Device Simulation Based on Bulk Monte Carlo Data," *J. Appl. Phys.* **97**(9), 093710 (2005).

[4] M. Vasicek *et al.*, "Parameter Modeling for Higher-Order Transport Models in UTB SOI MOSFETs," in *Proc. 12th IWCE* (2007) 96–97.

[5] B. Neinhüs *et al.*, "A CPU Efficient Electron Mobility Model for MOSFET Simulation with Quantum Corrected Charge Densities," in *Proc.ESSDERC* (2000) 332–335.

[6] G. Karlowatz *et al.*, "Full-Band Monte Carlo Analysis of Electron Transport in Arbitrary Strained Silicon," in *Proc. SISPAD* (2006) 600–604.

[7] M. Karner *et al.*, "VSP - A Multi-Purpose Schrödinger-Poisson Solver for TCAD Applications," in *Proc. 11th IWCE* (2006) 255–256.

[8] M. Lundstrom, *Fundamentals of Carrier Transport* X of *Modular Series on Solid State Device*, Addison-Wesley (1990).

[9] K. Blotekjaer, "Transport Equations for Electrons in Two-Valley Semiconductors," *IEEE Transactions on Electron Devices* **ED-17**(1), 38 (1970).

[10] T. Grasser, "Non-Parabolic Macroscopic Transport Models for Semiconductor device simulation," *PhysicaA* **349**(1/2), 221 (2005).

[11] T. Grasser *et al.*, "Using Six Moments of Boltzmann's Transport Equation for Device Simulation," *J. Appl. Phys.* **90**(5), 2389 (2001).

[12] M. Vasicek *et al.*, "Modeling of Macroscopic Transport Parameters in Inversion Layers," in *Proc. ISDRS* (2007).

[13] www.iue.tuwien.ac.at, "Minimos-NT 2.0 User's Guide," (2002).

[14] S.-I. Takagi *et al.*, "On the Universality of Inversion Layer Mobility in Si MOSFET's: Part I–Effects of Substrate Impurity Concentration," **41**(12), 2357 (1994).

[15] A. Khakifirooz and D. Antoniadis, "On the Electron Mobility in Ultrathin SOI and GOI," *EDL* **25**(2), 80 (2004).